Published in "Physical Review A 81(1): 012501, 2010"
which should be cited to refer to this work.

Synchrotron-radiation-based determination of Xe L-subshell Coster-Kronig yields: A reexamination via high-resolution x-ray spectroscopy

W. Cao,[1,*] J.-Cl. Dousse,[1] J. Hoszowska,[1] M. Žitnik,[2] M. Kavčič,[2] and K. Bučar[2]
[1]*Department of Physics, University of Fribourg, Ch-1700 Fribourg, Switzerland*
[2]*J. Stefan Institute, SI-1001 Ljubljana, Slovenia*

The xenon L-subshell Coster-Kronig (CK) transition yields were revisited via high-resolution measurements of the $L\alpha_{1,2}$ ($L_3 - M_{4,5}$) and $L\beta_1$ ($L_2 - M_4$) x-ray emission lines. The L x-ray spectra were measured employing a Johansson-type curved crystal spectrometer and energy-tunable synchrotron radiation. The CK yields were derived from the relative L x-ray intensity jumps at the L edges by fitting the fluorescence intensities as a function of the photon energy to the L-subshell photoionization cross sections. The latter were obtained from the measured L-edge photoabsorption spectrum. Values of 0.118 ± 0.029, 0.383 ± 0.037, and 0.096 ± 0.016 were found for the f_{23}, f_{13}, and f_{12} CK yields, respectively. Thanks to high resolution, the L_1 fluorescence yield of 0.059 ± 0.002 was also determined from intensity ratios of the well-resolved $L\beta_4$ ($L_1 - M_2$) and $L\beta_1$ ($L_2 - M_4$) lines.

PACS number(s): 32.70.−n, 32.80.Hd, 32.50.+d, 32.30.Rj

I. INTRODUCTION

The decay scheme of atomic inner-shell vacancies is branched into cascades of radiative and nonradiative Auger transitions. The Coster-Kronig (CK) transitions are the fastest Auger transitions, in which the vacancy transfers within the same major shell. The vacancy transfer probability from the i subshell to the higher j subshell is called the CK yield f_{ij}. CK rates depend on the initial- and final-state wave functions and are very sensitive to electron binding energies as well as to solid-state effects [1,2].

Particularly interesting is the region around $Z = 48$ where a sharp decrease in the f_{13} value is expected due to the $L_1 - L_3M_{4,5}$ transitions becoming energetically forbidden. Large discrepancies between the theoretical [2,3] and existing experimental results [4,5] point out the need for new accurate data. Experimental determination of the L-shell CK yields presents, however, considerable difficulties. For this reason, data are scarce and often suffer from large uncertainties [6]. To date, to determine the f_{23} yields, mostly the $K\alpha$-L x-ray coincidence method [6,7] was used. This technique, however, fails in the case of the L_1-subshell CK yields due to the dipole forbidden $K - L_1$ radiative transition. The alternative photoionization experimental method was limited to the use of radionuclides [8].

The subshell-selective photoionization method based on energy-tunable monochromatic synchrotron radiation [9] offers the possiblity to measure all L-subshell CK yields. This method has been successfully applied to determine CK yields for solids [9–13] as well as for Xe [14]. So far, most measurements of the x-ray fluorescence lines were performed by means of energy-dispersive semiconductor detectors. In our recent work on Pd ($Z = 46$) [15], the subshell-selective photoionization method was combined with high-resolution x-ray spectroscopy, allowing even the partial $L_1 - L_3M_{4,5}$ CK yield to be deduced. By applying this technique to elements within the mid-Z region, it would certainly be possible to reveal the L_1 CK yield cutoff trend.

In this article, we report on the revisit of the L-subshell f_{23}, f_{13}, and f_{12} CK yields for xenon ($Z = 54$) via the synchrotron-radiation-based high-resolution x-ray spectroscopy technique. The individual L-subshell photoionization cross sections were determined from the measured x-ray-absorption spectrum. The measurements of the $L\alpha_{1,2}$ ($L_3 - M_{4,5}$) and $L\beta_1$ ($L_2 - M_4$) lines were carried out by means of a high-resolution, Johansson-type crystal x-ray spectrometer. The CK yields were derived from the variation of the $L\alpha_{1,2}$ and $L\beta_1$ fluorescence-line intensities at the absorption L edges due to the onsets of CK vacancy transfers. In addition, the L_1-subshell fluorescence yield ω_1 was also determined from intensity ratios of the well-resolved $L\beta_4$ and $L\beta_1$ lines.

II. EXPERIMENT

The measurements were performed at the x-ray absorption fine structure (XAFS) beamline of Elettra synchrotron in Trieste, Italy, employing the x-ray spectrometer of the Jožef Stefan Institute [16]. The primary x-ray beam was monochromatized by means of a double-crystal Si(111) monochromator, and higher harmonics were reduced with a Pt-coated mirror. The photon flux incident on the Xe sample was $\sim 10^{10}$ photons/s. The Xe gas was contained in a 10-mm-long stainless-steel cell sealed with 12.5-μm-thick Kapton foils. Two ionization chambers, one in front and one after the spectrometer, were used for the absorption measurements and also for normalization purposes. The experimental setup was similar to the one described in [17].

For the absorption measurement, the Xe gas pressure was kept at a nominal value of 500 mbar. In order to obtain both a high enough photon beam transmission and detector efficiency, the percentages and pressures of the helium-nitrogen gas mixtures for each of the ionization chambers were optimized. The photon energy was tuned with 0.2-eV steps in the range from 4500 to 5800 eV. Another scan over the same energy range was performed with an empty target cell in

*wei.cao@unifr.ch

order to determine the residual attenuation in the Kapton windows and in the ionization chambers. For the fluorescence measurements, the Xe gas pressure was 200 mbar.

The L x-ray fluorescence lines of Xe were measured at an angle of 90° with respect to the horizontally polarized incident photon beam. A cylindrically curved quartz $(10\bar{1}0)$ crystal in the second order of reflection was employed. The diffracted x rays were recorded with a thermoelectrically cooled (−40°C), back-illuminated CCD camera consisting of 770×1153 pixels with a pixel size of $22.5 \times 22.5\ \mu m^2$. The x-ray spectrometer energy resolution was about 0.2 eV. For normalization purposes, the incident photon flux was recorded online with the first ionization chamber each 10 s. Beam intensities were corrected for absorption in the ionization chamber and the Kapton windows in the beam path.

The fluorescence spectra were calibrated using the reference energies of the $L\alpha_1$ (or $L\beta_1$) x-ray line reported in Ref. [18]. Depending on the incident photon energy and the total photon number, the time to collect an L x-ray spectrum varied from 50 to 170 min. A series of 14 $L\alpha$ and another series of 7 $L\beta_1$ x-ray emission spectra were recorded. The incident-beam energy was tuned from 4850 eV (68 eV above the L_3-edge E_3) to 5700 eV (247 eV above the L_1-edge E_1) for the measurements of the $L\alpha$ lines and from 5200 eV (96 eV above the L_2-edge E_2) to 5750 eV (297 eV above E_1) for the $L\beta_1$ and $L\beta_4$ lines.

III. DATA ANALYSIS

A. Spectra fitting

The Xe $L\alpha$ and $L\beta_1$ x-ray spectra measured at two different photon energies are shown in Figs. 1 and 2, respectively. It can be seen that the high-resolution x-ray emission spectroscopy employed in our work permits us to resolve the individual

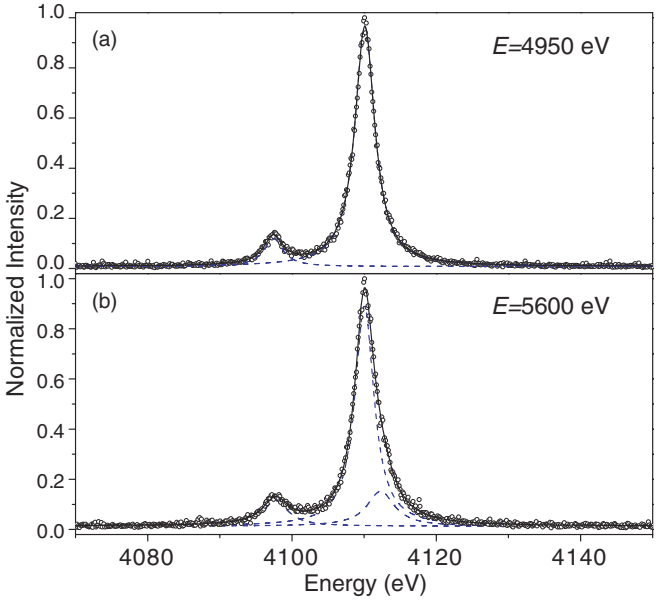

FIG. 1. (Color online) Fitted high-resolution $L\alpha$ x-ray spectra of Xe at different incident-beam energies: (a) $E = 4950$ eV and (b) $E = 5600$ eV. Solid thick lines represent the total fit to the experimental data (dots) and dashed lines the individual components.

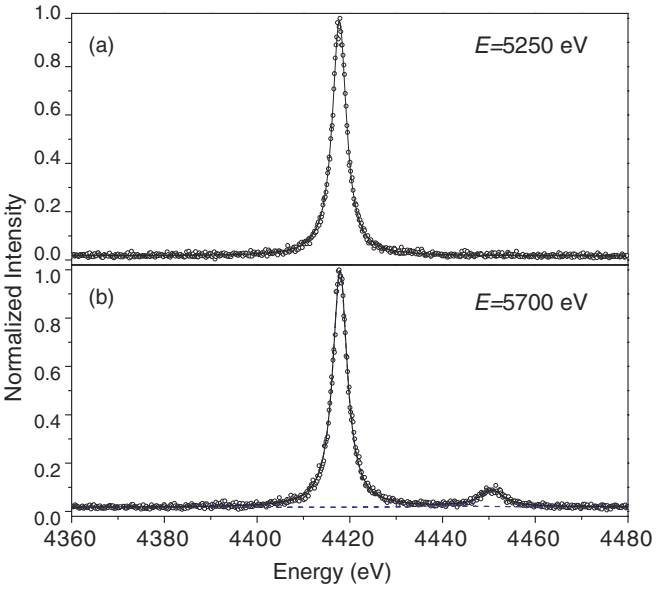

FIG. 2. (Color online) Fitted high-resolution $L\beta_1$ $(L_2 - M_4)$ x-ray spectra of Xe at different incident-beam energies: (a) $E = 5250$ eV and (b) $E = 5700$ eV. Solid thick lines represent the total fit to the experimental data (open circles) and dashed lines the individual components. In (b), the peak on the high-energy side of the $L\beta_1$ line corresponds to the $L\beta_4$ $(L_1 - M_2)$ transition.

$L\alpha$ (or $L\beta$) x-ray transitions, thus avoiding an elaborate fitting procedure such as is needed in the case of L-x-ray spectra measured with energy-dispersive detectors [13]. In inner-shell photoionization, however, the diagram transitions may be accompanied by satellite lines resulting from additional vacancies present in outer subshells via Coster-Kronig and shake [19] processes. Due to the reduced screening of the nuclear charge, the x-ray satellite lines are shifted in energy with respect to the diagram transitions.

Multiconfiguration Dirac-Fock calculations [20] show that the first-order N and O satellites are not resolved from the $L\alpha$ and $L\beta_1$ parent lines. This overlap of the LN and LO satellite transitions with the parent diagram lines results in a nonlifetime broadening of the latter. Our calculations, performed within the framework of the sudden approximation model using self-consistent Dirac-Fock wave functions from the code of reference [20], predict for the O-shake probability a value of 0.14 and for the N-shake 0.05. Although the O-shell electron-shake contribution is non-negligible, the fluorescence intensity jumps are not affected because it is constant over the measured photon energy range. The same holds for the N-shell shake contribution. For incident-beam energies tuned above the L_1 edge, the opening of the $L_1 - L_3N$ CK channel results in an asymmetry on the high-energy flank of the $L\alpha_1$ line [see Fig. 1(b)]. The $L\alpha M$ satellite transitions, expected at ∼13 eV above the $L\alpha_1$ line, were not observed. This is not surprising because the $L_1 - L_3M$ CK transitions are energetically forbidden and the M-shake probability of 0.006 is negligibly small.

By taking these considerations into account, each $L\alpha_{1,2}$ line was fitted by two Lorentzians with widths as free parameters. Above the L_1 edge, an additional Lorentzian profile was needed to account for the $L\alpha_1 N$ satellite contribution. For

the $L\beta_1$ line as well as for the $L\beta_4$ ($L_1 - M_2$) line observed for photon impact energies tuned above the L_1 edge [see Fig. 2(b)], a single Lorentzian profile was used because the $L_1 - L_2N$ CK transitions are very weak. The fitted L x-ray intensities were normalized to the same incident photon flux and data acquisition time. In addition, each spectrum collected at an incident energy E was weighted by the corresponding beam-absorption correction factor

$$F_{\rm corr}(E) = \frac{\mu(E)b}{1 - \exp[-\mu(E)b]}, \tag{1}$$

which is valid for a perpendicular experimental geometry [21]. The total attenuation $\mu(E)b$, where b stands for the interaction path, was measured at a target gas pressure of 200 mbar in the beam energy range 4500 eV $\leqslant E \leqslant$ 5800 eV with 1-eV steps.

B. *L*-subshell cross-section parametrization

The experimental $L\alpha$ fluorescence intensity $I(E)$ is proportional to the total L x-ray production cross section

$$\sigma^X_{L\alpha}(E) = \omega_{L\alpha}[\sigma_3(E) + f_{23}\sigma_2(E) + (f_{13} + f_{12}f_{23} + f'_{13})\sigma_1(E)], \tag{2}$$

where $\sigma_i(E)$ are the L_i ($i = 1, 2,$ or 3) subshell photoionization cross sections and f'_{13} denotes the L_1 to L_3 hole transfer rate resulting from the $L_1 - L_3$ radiative transition. The $\omega_{L\alpha}$ stands for the $L\alpha$ diagram-line fluorescence yield. Similarly, the $L\beta_1$ and the $L\beta_4$ x-ray production cross sections are

$$\sigma^X_{L\beta_1}(E) = \frac{\Gamma_{L\beta_1}}{\Gamma_2}[\sigma_2(E) + f_{12}\sigma_1(E)] \tag{3}$$

and

$$\sigma^X_{L\beta_4}(E) = \frac{\Gamma_{L\beta_4}}{\Gamma_1}\sigma_1(E) = \frac{\Gamma_{L\beta_4}}{\Gamma_1^{\rm rad}}\omega_1\sigma_1(E), \tag{4}$$

respectively. $\Gamma_{L\beta_1}$ and $\Gamma_{L\beta_4}$ represent the fluorescence widths of the two transitions, Γ_1 and Γ_2 the total widths of the L_1 and L_2 subshells, and $\Gamma_1^{\rm rad}$ the radiative width of the L_1 subshell.

In order to derive the CK yields from the measured L x-ray fluorescence intensities, the variation of the photoionization cross sections with photon energy should be known. It is generally assumed that within a certain energy range, the cross sections vary smoothly with photon energy and the dependence can be described by a power law. According to the independent particle approximation (IPA) calculations, the single L_i-subshell photoionization cross section σ_i for Xe can be expressed as

$$\sigma_i(E) = a_i E^{b_i}, \tag{5}$$

where a_i is in the unit of Mbarn and E in keV.

The Xe L-shell photoionization cross sections are shown in Fig. 3. Because the temperature and pressure of Xe in the gas cell could not be determined accurately, the measured Xe L-edge absorption spectrum was normalized to the L_3-pre-edge x-ray absorption coefficients reported by Wuilleumier [22]. The L_3-pre-edge attenuation coefficients were fitted with the power law and extrapolated in order to get the total L-shell photoionization cross section.

Below the L_2 edge, the L_3-subshell ionization cross section is given by the measured total L-shell photoionization cross section. The latter is depicted by circles in Fig. 3 and compared to the power-law dependence of Jitschin *et al.* [14] shown by the dashed line. Obvious deviations of our experimental values from those based on the IPA calculations are observed. These differences could be due to many-body and multi-ionization effects. However, in the region slightly below the L_2 edge, the slopes of our experimental and IPA theoretical curves match each other quite well. Thus, adopting for the parameter b_3 the value of Jitschin *et al.* [14], the curve given by Eq. (5) was just scaled down to match the experimental points before the L_2 edge. Above the L_2 edge, the rescaled power-law curve was used to extrapolate the L_3-subshell cross section which was then subtracted from the experimental values to get the L_2 and L_2- plus L_1-subshell cross sections for incident-beam energies $E_2 < E < E_1$ and $E > E_1$, respectively. Similarly, the L_1-subshell cross section was obtained by subtracting the extrapolated values from the rescaled power-law curve for the L_2-subshell cross section. The parameters a_i of the rescaled extrapolation curves together with the parameters a_i and b_i of Jitschin *et al.* [14] are listed in Table I. The fitted curves are depicted with solid lines in Fig. 3.

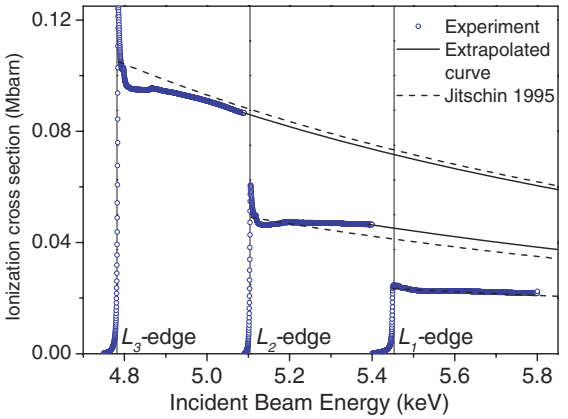

FIG. 3. (Color online) Experimental and theoretical L-subshell photoionization cross sections of Xe. The solid lines are the extrapolated curves obtained by scaling the analytical expression given by Eq. (5) to the measured values (open circles). The dashed lines are the theoretical values given by Jitschin *et al.* [14].

IV. RESULTS AND DISCUSSION

The method used to get the CK yields for Xe is similar to the one reported in our previous work [15]. The f_{23} CK yield was extracted from the $L\alpha$ intensity jump at the L_2 edge. First, the fluorescence intensity below the L_2 edge was fitted with

TABLE I. The fitting parameters for the power-law dependence of the L_i-subshell ($i = 3, 2, 1$) photoionization cross sections.

Parameter	i		
	3	2	1
a_i (Mbarn)	7.640	4.076	–
a_i [14] (Mbarn)	7.818	3.716	0.467
b_i [14]	−2.753	−2.654	−1.765

the following expression:

$$I_3(E) = C\omega_{L\alpha}\sigma_3(E), \tag{6}$$

where C is the instrumental proportionality constant. From the fit, the parameter $A_3 = C\omega_{L\alpha}$ was obtained. To derive the CK contribution, the fluorescence intensities $I_3(E)$ for energies above the L_2 edge were extrapolated and subtracted from the $I(E)$ data. For incident-beam energies between the L_2 and L_1 edges, the values

$$I_2(E) = I(E) - I_3(E) \tag{7}$$

correspond to the additional fluorescence intensities due to the $L_2 - L_3$ CK process. From the fit of $I_2(E)$, the parameter $A_2 = f_{23}C\omega_{L\alpha}$ was obtained. Finally, the f_{23} CK rate was derived from the ratio of A_2 to A_3:

$$f_{23} = \frac{A_2}{A_3}. \tag{8}$$

Similarly, the f_{13} CK yield can be expressed as

$$f_{13} = \frac{A_1}{A_3} - f_{12}f_{23}, \tag{9}$$

where the f_{12} yield is given by the $L\beta_1$ intensity jump at the L_1 edge:

$$f_{12} = \frac{A_1'}{A_2'}. \tag{10}$$

Here, A' is introduced to distinguish the $L\alpha$ and $L\beta_1$ intensities. The fitting parameters for the $L\beta_1$ line intensities are $A_2' = C'\omega_{L\beta_1}$ and $A_1' = f_{12}C'\omega_{L\beta_1}$, where the instrumental proportionality constant is C' due to the changes of the crystal and detector positions. The term f_{13}' is omitted in Eq. (9) because the competing intrashell radiative transition $L_1 - L_3$ is negligibly weak compared to the CK process [12].

Results of the fitting procedure for the $L\alpha$ intensities are presented in Fig. 4. Values of 0.118 ± 0.029, 0.383 ± 0.037, and 0.096 ± 0.016 were found for the f_{23}, f_{13}, and f_{12} CK yields, respectively. They are listed in the first row of Table II. For comparison, CK yields adopted in the former work [14] are listed in the second row. The theoretical predictions given

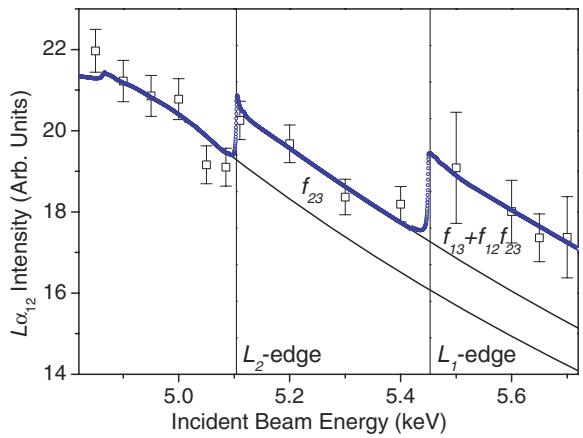

FIG. 4. (Color online) The $L\alpha_{1,2}$ x-ray fluorescence intensities (open squares) fitted with the measured photoionization cross sections (open circles). The solid lines show the corresponding extrapolated power-law curves.

TABLE II. Coster-Kronig rates and the L_1 fluorescence yield for Xe.

	f_{23}	f_{13}	f_{12}	ω_1
Present	0.118(29)	0.383(37)	0.096(16)	0.059(2)
Jitschin [14]	0.14(2)	0.23(4)	0.12(3)	–
Chen [2]	0.174	0.328	0.196	0.048
Campbell [6]	0.159(40)	0.25(8)	–	–
Krause [23]	0.154(31)	0.28(4)	0.19(4)	0.046(9)
Jitschin [14][a]	0.115	0.185	0.095	–
Jitschin [14][b]	0.174	0.316	0.169	–

[a]Results with electron correlation corrections.
[b]Results without electron correlation corrections.

by Chen *et al.* [2], the values recommended by Campbell [6], and the semiempirical values reported by Krause [23] are also quoted. Our data for the f_{12} and f_{23} are in general smaller than the values from theoretical and semiempirical predictions but are consistent with the values adopted by Jitschin *et al.* [14]. For the f_{13} CK rate, however, the listed values in Table II differ: Our value is closer to the one reported by Chen *et al.* [2], while the result from the work of Ref. [14] is closer to the one by Campbell [6]. To make a detailed comparison with the former work of Jitschin *et al.* [14], data with and without electron correlation corrections [14] are also presented in the table. The current value for f_{13} is found to be closer to the result obtained in [14] from the IPA fit but much larger than the one with correlation corrections.

In order to get a more general view of the Z dependence for the f_{13} yield in this Z region, the f_{13} CK probabilities for Xe and the existing experimental results for neighboring elements Mo ($Z = 42$) [12], Pd ($Z = 46$) [15], and Ag ($Z = 47$) [12,24], and the recent results for Ba ($Z = 56$) [25] and La ($Z = 57$) [26] are compiled in Fig. 5. It can be seen that

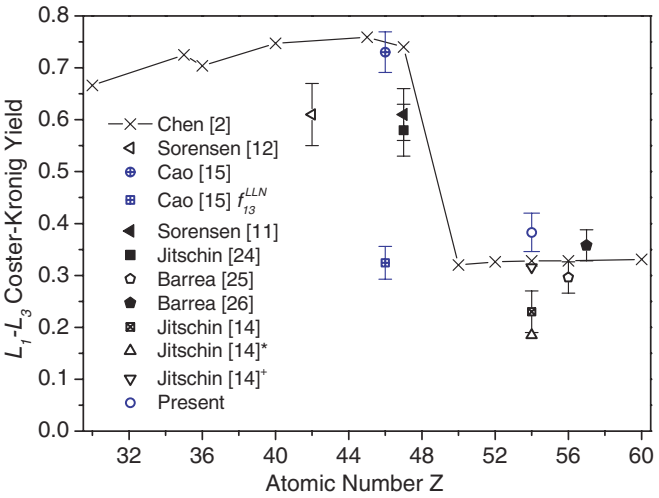

FIG. 5. (Color online) Present f_{13} CK rate of Xe (open circle). The datum is compared to theoretical values from [2], the available experimental data for the neighboring elements, Mo [12], Pd [15], Ag [11,24], Ba [25], and La [26], and for Xe [14] to the adopted value, as well as to values with ($*$) and without ($+$) electron correlation corrections. The f_{13}^{LLN} denotes the Pd partial $L_1 - L_3N$ CK yield obtained in [15].

our result is in reasonable agreement with values for higher Z elements (Ba and La) and with the partial $L_1 - L_3N$ yield for Pd.

Differences among the f_{13} CK yield values can be attributed mainly to the determination of the L_i-subshell photoionization cross sections. Limitations of the IPA model can be clearly seen in Fig. 3. The discrepancies between the IPA model and the fit to our experimental data could be due to multiple ionization processes [27,28], electron correlation effects [29,30], quantum interferences between one- and two-electron excitation processes [31], or the dynamic screening effects [32]. Calculations including these effects could lead to a more precise total L-shell photoionization cross section. This is an issue still under debate [33], which is, however, beyond the scope of our work.

When the energy of the photon beam is tuned above the L_1 edge, both $L\beta_1$ and $L\beta_4$ transitions are observed in the measured spectrum [see Fig. 2(b)]. The intensity ratio of these two close-lying lines can be accurately calculated, giving the possibility to determine the ω_1 fluorescence yield. This method is straightforward and free from elaborate spectrometer efficiency corrections [7,34]. Using Eqs. (3) and (4), the L_1-subshell fluorescence yield is given by

$$\omega_1 = \frac{I_{L\beta_4}}{I_{L\beta_1}} \frac{\Gamma_{L\beta_1}}{\Gamma_{L\beta_4}} \frac{\Gamma_1^{\rm rad}}{\Gamma_2} \frac{[f_{12}\sigma_1(E) + \sigma_2(E)]}{\sigma_1(E)}. \qquad (11)$$

By adopting for $\Gamma_{L\beta_1}$ and $\Gamma_{L\beta_4}$ the interpolated values of Campbell and Wang [35], and for the $\Gamma_1^{\rm rad}$ and Γ_2 the calculations of Chen *et al.* [2], ω_1 was found to be 0.059 ± 0.002. This result is higher than the theoretical predictions of Chen *et al.* [2] and Krause [23] and smaller than the value of 0.068 ± 0.007 determined for Ba ($Z = 56$) [25].

V. CONCLUSION

We have determined the Coster-Kronig transition yields for Xe via synchrotron-radiation-based high-resolution measurements of the L x-ray emission lines. By making use of the measured L-subshell photoionization cross sections and the power-law dependence of the photoionization cross sections on the primary photon energy, the f_{23} and f_{13} CK yields were derived from the relative $L\alpha$ intensity jumps at the L edges and the f_{12} rate from the $L\beta_1$ intensity jump at the L_1 edge. From the intensity ratios of the $L\beta_4$ and the $L\beta_1$ lines, the fluorescence yield of the L_1 subshell was also determined.

Our results for the f_{12} and f_{23} CK yields were found to be consistent with those of Jitschin *et al.* [14], whereas for the f_{13} rate, a higher value was obtained. The discrepancy was mainly attributed to the different parameterization of the L_i photoionization cross sections and, in particular, to the limitations of the IPA model used by Jitschin *et al.*. Indeed, the multiple-electron excitation and many-body and time-dependent effects, which are implicitly included in our measured photoionization cross sections, were neglected in the IPA theoretical predictions. To further reduce the uncertainty of the CK values, more elaborate calculations would be needed. Experimentally, coincidence measurements between the CK electron and the photon or Auger electron emitted in the subsequent decay would allow the separation of the L_3 and L_2 photoionization cross sections above the L_2 and L_1 thresholds, respectively.

ACKNOWLEDGMENTS

We wish to acknowledge L. Olivi for the beamline operation during the experiments. This project was financially supported by the Swiss National Science Foundation (Grant No. 200020-125124) and the program of the Slovenian Research Agency (Program No. P1-0112).

[1] W. Bambynek, B. Crasemann, R. W. Fink, H.-U. Freund, H. Mark, C. D. Swift, R. E. Price, and P. V. Rao, Rev. Mod. Phys. **44**, 716 (1972).
[2] M. H. Chen, B. Crasemann, and H. Mark, Phys. Rev. A **24**, 177 (1981).
[3] S. Puri, D. Mehta, B. Chand, N. Singh, and P. N. Trehan, X-ray Spectrom. **22**, 358 (1993).
[4] B. L. Doyle and S. M. Shafroth, Phys. Rev. A **19**, 1433 (1979).
[5] E. Rosato, Nucl. Instrum. Methods Phys. Res. B **15**, 591 (1986).
[6] J. L. Campbell, At. Data Nucl. Data Tables **85**, 291 (2003).
[7] R. W. Dunford, E. P. Kanter, B. Krässig, S. H. Southworth, L. Young, P. H. Mokler, Th. Stöhlker, S. Cheng, A. G. Kochur, and I. D. Petrov, Phys. Rev. A **74**, 062502 (2006).
[8] J. L. Campbell, At. Data Nucl. Data Tables **95**, 115 (2009), and references therein.
[9] W. Jitschin, G. Materlik, U. Werner, and P. Funke, J. Phys. B **18**, 1139 (1985).
[10] U. Werner and W. Jitschin, Phys. Rev. A **38**, 4009 (1988).
[11] S. L. Sorensen, R. Carr, S. J. Schaphorst, S. B. Whitfield, and B. Crasemann, Phys. Rev. A **39**, 6241 (1989).
[12] S. L. Sorensen, S. J. Schaphorst, S. B. Whitfield, B. Crasemann, and R. Carr, Phys. Rev. A **44**, 350 (1991).
[13] R. A. Barrea, C. A. Pérez, and J. Sánchez, J. Phys. B: At. Mol. Opt. Phys. **35**, 3167 (2002).
[14] W. Jitschin, R. Stötzel, T. Papp, M. Sarkar, and G. D. Doolen, Phys. Rev. A **52**, 977 (1995).
[15] W. Cao, J. Hoszowska, J.-Cl. Dousse, Y. Kayser, M. Kavčič, M. Žitnik, K. Bučar, A. Mihelič, J. Szlachetko, and K. Słabkowska, Phys. Rev. A **80**, 012512 (2009).
[16] M. Kavčič, A. G. Karydas, and Ch. Zarkadas, Nucl. Instrum. Methods Phys. Res. B **222**, 601 (2004).
[17] M. Žitnik, M. Kavčič, K. Bučar, A. Mihelič, M. Štuhec, J. Kokalj, and J. Szlachetko, Phys. Rev. A **76**, 032506 (2007).
[18] R. D. Deslattes, E. G. Kessler, Jr., P. Indelicato, L. de Billy, E. Lindroth, and J. Anton, Rev. Mod. Phys. **75**, 35 (2003).
[19] T. Åberg, Phys. Rev. **156**, 35 (1967).
[20] K. G. Dyall, I. P. Grant, C. T. Johnson, F. A. Parpia, and E. P. Plummer, Comp. Phys. Comm. **55**, 425 (1989).
[21] F. Gel'mukhanov and H. Ågren, Phys. Rep. **312**, 87 (1999).
[22] F. Wuilleumier, Phys. Rev. A **6**, 2067 (1972).

[23] M. O. Krause, J. Phys. Chem. Ref. Data **8**, 307 (1979).
[24] W. Jitschin, R. Stötzel, T. Papp, and M. Sarkar, Phys. Rev. A **59**, 3408 (1999).
[25] R. A. Barrea, C. A. Pérez, and J. Sánchez, Nucl. Instrum. Methods Phys. Res. B **215**, 308 (2004).
[26] R. A. Barrea, C. A. Pérez, and J. Sánchez, Spectrochem. Acta B **58**, 51 (2003).
[27] I. Arčon, A. Kodre, M. Štuhec, D. Glavič-Cindro, and W. Drube, Phys. Rev. A **51**, 147 (1995).
[28] Y. Ito, A. M. Vlaicu, T. Tochio, T. Mukoyama, M. Takahashi, S. Emura, and Y. Azuma, Phys. Rev. A **57**, 873 (1998).
[29] W. Jitschin and R. Stötzel, Phys. Rev. A **58**, 1221 (1998).
[30] A. Zangwill and P. Soven, Phys. Rev. A **21**, 1561 (1980).
[31] K. Zhang, E. A. Stern, J. J. Rehr, and F. Ellis, Phys. Rev. B **44**, 2030 (1991).
[32] A. L. Ankudinov, A. I. Nesvizhskii, and J. J. Rehr, Phys. Rev. B **67**, 115120 (2003).
[33] S. Botti, A. Schindlmayr, R. Del Sole, and L. Reining, Rep. Prog. Phys. **70**, 357 (2007).
[34] T. Papp, J. L. Campbell, and S. Raman, Phys. Rev. A **49**, 770 (1994).
[35] J. L. Campbell and J.-X. Wang, At. Data Nucl. Data Tables **43**, 281 (1990).